2017 IEEE International Conference on Robotics and Automation (ICRA)
Singapore, May 29 - June 3, 2017

Visual Tracking of Multiple Moving Targets in 2D Ultrasound Guided Robotic Percutaneous Interventions

Mert Kaya, Enes Senel, Awais Ahmad, and Ozkan Bebek

Abstract— **Percutaneous needle procedures are mostly carried out with the guidance of 2D ultrasound (US) imaging. US images are inherently noisy and their resolutions are low. Hence, target tracking can be challenging. Image based tracking methods can be used to track the needle and the target. This paper proposes visual tracking of multiple moving points, such as biopsy needles and targets, in 2D US images using normalized cross correlation and mutual information similarity functions. Both moving and deformable targets can be tracked. An affine motion model is used for small and moving target tracking and a thin plate spline motion model is used for deformable target tracking. During the tracking, needle and target template images are updated with a template update strategy. Also, tracking outputs of normalized cross correlation and mutual information are fused using the Kalman filter to reduce the tracking error. During the experiments, needle is inserted using a needle insertion robot. 2D US probe is attached to a robotic arm's end effector to servo the probe along the needle insertion path. Proposed needle and target tracking methods were tested with phantoms. Accuracies of the needle tip and moving target tracking methods were measured using an optical tracking system. Experimental results showed that the proposed tracking method could be used to simultaneously track the needle tip and the targets in real-time in 2D US guided percutaneous needle procedures.**

I. INTRODUCTION

Biopsy is extraction of live tissue for examination of a disease. During these operations, a needle is inserted manually or with the assistance of a robot. Robot assisted biopsy procedure is a reliable way to reach the target tissue. Indeed, the needle trajectory can be preplanned and robots can move with high resolution. The insertions are done with the help of medical imaging devices that image the needle and the target tissue. Success of the biopsy is linked to the positioning of the needle. If the needle is not inserted with the correct trajectory, target tissue can be missed. Also, with every insertion tissue damage occurs. For the success of the operation tracking of the target tissue as well as the needle tip is needed. Target can move due to the internal forces or movement of the imaging probe [1]. If the target is missed, sample can be taken from irrelevant places.

This work was supported by the Scientific and Technical Research Council of Turkey (TUBITAK) under Grant No. 112E312.

Mert Kaya and Awais Ahmad are with Department of Electrical and Electronics Engineering, Ozyegin University, Cekmekoy, 34794 Istanbul, Turkey. e-mail: mert.kaya@ozu.edu.tr; awais.ahmad@ozu.edu.tr

Enes Senel is with the Department of Computer Science, Ozyegin University, Cekmekoy, 34794 Istanbul, Turkey. e-mail: enes.senel@ozu.edu.tr

Ozkan Bebek is with the Department of Mechanical Engineering, Ozyegin University, Cekmekoy, 34794 Istanbul, Turkey. e-mail: ozkan.bebek@ozyegin.edu.tr

Among the medical imaging devices, 2D US imaging is the most commonly used method. US imaging does not have any known side effects. Also, tissue can be imaged using a small hand held probe. Thus, it provides large work space for both operators and robots. But, US images suffer from low signal-to-noise ratio and they contain excessive number of artifacts. Hence, the needle and the target tissue tracking can be challenging. Visual tracking techniques can be used to simultaneously track the target and the needle during the biopsy procedures. This study proposes simultaneous visual tracking of the needle and the targets for both manual and robotic assisted interventions.

In the literature, several methods were developed to track either the needle tip or the target tissue in both 2D and 3D US images. Mathiassen *et al.* [2] developed a method to track the needle tip in 2D US images. First, needle axis was localized and then its tip was estimated. Localized needle tip coordinates were tracked using Kalman and particle filters. Ayvali and Desai [3] detected the needle tip using circular Hough transform. Detected needle tip points were tracked using optical flow method. Zhao *et al.* [4] segmented and tracked the needle tip in 3D US images. Needle pixels were segmented using Frangi's vesselness filter. Then, the filtered image was binarized using a thresholding strategy. Needle axis and its tip were localized using RANSAC line fitting and localized needle tip points were tracked using Kalman filter.

Chatelain *et al.* [5] developed a method to localize and track the needle tip in 3D US images. First, needle insertion was detected using volumetric frame differences. After, needle insertion was detected, needle axis and its tip were localized using RANSAC line fitting. Localized needle tip points were tracked using Kalman filter. Also, the authors attached 3D US probe was onto a robotic arm to servo the US probe along the needle path. Chatelain *et al.* [6] developed a needle tip tracking method for 3D US guided robotic needle steering. 3D US probe was attached onto a robotic arm and the needle was inserted using another robotic arm. Bayesian framework was used to track the needle tip during the steering process. Vrooijink *et al.* [7] developed a robotic system for 2D US guided percutaneous needle procedures. The authors placed the US probe perpendicular to the needle and the US probe was servoed along the needle path. In order to detect the needle tip, circular hough transform was used and localized needle tip points were tracked using Kalman filter.

Royer *et al.* [8] tracked the deformable targets in 3D US images in real-time without using any fiducial markers. They

combined both displacement and physical models of tissues to track the target. Royer *et al.* [9] tracked both rigid and non-rigid targets in 2D US images. They distinguished the rigid and non-rigid motions using image modality. After motion was distinguished, hierarchical grid interpolation method was used to track targets.

In our previous studies, Gabor filter was used to segment the needle pixels in 2D US images [10] and needle tip was estimated with a probability mapping method [11] and it was tracked in real-time using the Kalman filter [12]. Needle tip is also visually tracked using sum of squared differences and sum of conditional variances [13]. During the tracking, needle loss was also detected using normalized cross correlation.

In the literature review provided above, studies included the tracking of either the needle or the target in US images. Simultaneous tracking of both is required since target can also move during the needle insertion. To overcome this shortcoming, simultaneous visual tracking of the needle and the target is proposed. The main difference between proposed tracking method and the other tracking methods is that the needle tip and the target are simultaneously tracked using only the motion information acquired from the US image.

US images contain significant motion information while the needle is inserted. Once the needle and the target are localized, this motion information can be used for tracking. An example motion analysis while the needle is inserted towards the target is shown in Fig. 1. Lukas-Kanade optical flow method is used to analyze the motion [14]. Tissue shift is plotted as the vector field and overlaid onto the current frame in Fig.1-b. The motion information can be used to improve tracking of the needle and the target. Point based tracking methods, such as the Kalman filter, ignores the motion information in the image. Also, target and needle should be detected in every frame with the proposed methods in the literature, however the needle might not be detected in every frame. Also, detection of the needles and the targets can be time consuming.

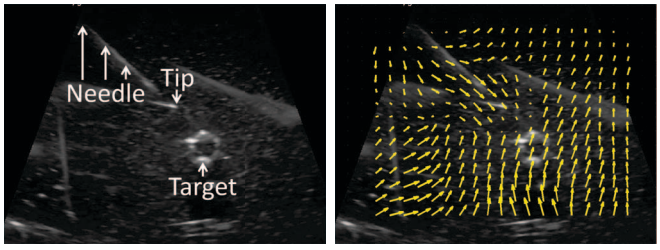

(a) Current Frame (b) Vector Field

Fig. 1: Motion analysis of a frame while the needle is inserted towards the target. (a) Current US frame. (b) Optical flow vector field is overlaid onto the current frame.

In this study, normalized cross correlation (NCC) and mutual information (MI) methods are used to track both moving and deformable targets. Affine motion model is used to track moving targets, and thin plate spline motion model is used to track deformable targets. Templates are updated with a template update strategy to prevent tracking failures. Also, tracking outputs of NCC and MI are fused to minimize the registration error during the tracking. To the best of our knowledge, this method is the first to simultaneously track the needle tip and the target in 2D US images using visual tracking methods. In the experiments, 2D US probe is attached to a robotic arm and the needle is inserted using a needle insertion robot. Needle tip is servoed along the needle path both in water tank and solid phantoms. In the following sections, visual tracking using NCC and MI for needle tip and target tracking is explained in detail.

II. Visual Tracking of Needle Tip

Visual tracking is the process of locating an object over time in frame sequences. Generally, the previous appearance of the object, defined as template image-$I_t(\mathbf{p})$ and current appearance of the object, defined as current image-$I_i(\mathbf{w}_{\mathrm{m}}(\mathbf{p};\mathbf{r}))$ are aligned to find its location in the current frame, where $\mathbf{p}$ vector contains $x-$ and $y-$ pixel coordinates of the current image [15]. This process is called image registration. $\mathbf{w}_{\mathrm{m}}(\mathbf{p};\mathbf{r})$ is known as the warping function and it transforms the vector $\mathbf{p}$. The aim of image registration is to find $\mathbf{r}$ vector which contains all motion parameters between current and template images. The process can be divided into consecutive two stages. In the first stage, similarity between an image pair is calculated. In the second stage, $\mathbf{r}$ is iteratively calculated. Iterations last until difference between two images reaches global minimum.

In order calculate the similarity, NCC or MI similarity functions can be used. These similarity functions are commonly used in medical image registration [16], [17]. Both of the similarity functions are robust to quick and significant intensity changes so they can be used to register an image pair in challenging conditions. The robustness of these similarity functions are evaluated with respect to nominal conditions and global intensity changes using reference image shown in Fig. 2-a. Reference image is captured while a needle is inserted into chicken breast. First template is cropped from the center of the reference template (see Fig. 2-b). In order to calculate the similarity value between the two images, first template is translated from -20 to 20 pixels with 1 pixel increments in $x-$ and $y-$axes. Similarity plots between the first template and the reference images are shown in the left column of Fig. 2. Second template is obtained by changing intensity values of the first template and it is shown in Fig. 2-c. As seen from Fig. 2-c, intensity values of the needle pixels are very close to the background pixels. Similarities between the second and the reference images are calculated and similarity plots are shown in the right column of Fig. 2. As seen from these similarity plots, NCC and MI values reach a global maximum value at the center even if the pixel intensities in the template image change significantly.

In the visual tracking of the needle tip, one of the most important steps is determining motion model of the needle. In our experiments, motion of the needle is translation motion model. It provides 2-DOF motion information ($\mathbf{r} =$

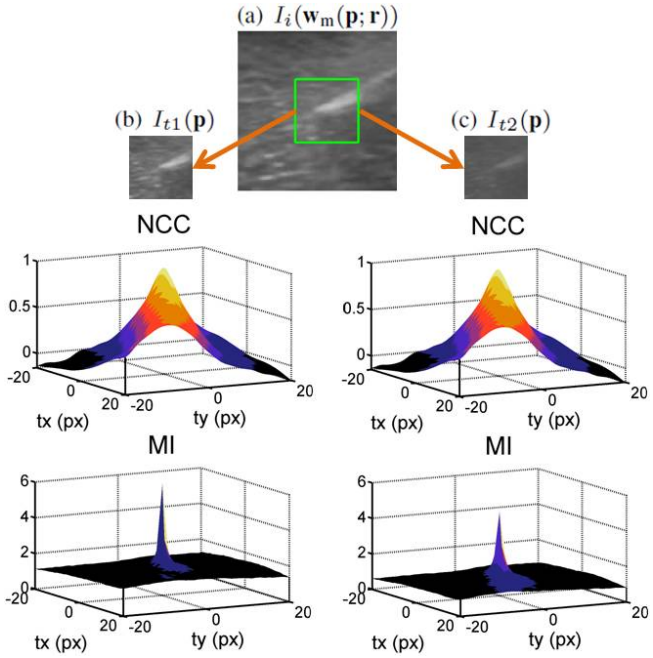

Fig. 2: 3D similarity plots between current and two template images using NCC and MI similarity functions. Left column contains similarity plots between (a) Current image, $I_i(\mathbf{w}_m(\mathbf{p};\mathbf{r}))$ and (b) 1^{st} Template. Right column contains similarity plots between (a) Current image, $I_i(\mathbf{w}_m(\mathbf{p};\mathbf{r}))$ and (b) 2^{nd} Template $I_{t2}(\mathbf{p})$.

r_1, r_2). But, needle template image contains both needle and surrounding tissue motion information. Although the needle is rigid, tissue deformation creates non-rigid motion components. Thus, affine motion model is chosen (1) for expressing motion model of the needle template, because it can be used to express the motion of both rigid and non-rigid tissue. Also, it provides 6-DOF motion information ($\mathbf{r} = r_1, ..., r_6$). In the rest of this section, calculation of $\mathbf{r}$ vector using NCC and MI similarity functions are explained.

$$\mathbf{w}_m(\mathbf{p};\mathbf{r}) = \begin{bmatrix} (1+r_1)\cdot x & + & r_3 \cdot y & + & r_5 \\ r_2 \cdot x & + & (1+r_4)\cdot y & + & r_6 \end{bmatrix} \quad (1)$$

A. Visual Tracking using NCC and MI

NCC value between $I_i(\mathbf{w}_m(\mathbf{p};\mathbf{r}))$ and $I_t(\mathbf{p})$ is computed as

$$NCC(\mathbf{r}) = \frac{\sum_{\mathbf{p}}(I_i(\mathbf{w}_m(\mathbf{p};\mathbf{r})) - \overline{I_i}) \cdot (I_t(\mathbf{p}) - \overline{I_t})}{\sqrt{\sum_{\mathbf{p}}(I_i(\mathbf{w}_m(\mathbf{p};\mathbf{r})) - \overline{I_i})^2} \cdot \sqrt{\sum_{\mathbf{p}}(I_t(\mathbf{p}) - \overline{I_t})^2}}$$

where $\overline{I_t}$ and $\overline{I_i}$ are mean values of the $I_t(\mathbf{p})$ and $I_i(\mathbf{w}_m(\mathbf{p};\mathbf{r}))$, respectively.

MI value between $I_i(\mathbf{w}_m(\mathbf{p};\mathbf{r}))$ and $I_t(\mathbf{p})$ is computed as

$$MI(\mathbf{r}) = \sum_{m,n} P_{I_i I_j}(m,n,\mathbf{r}) \log\left(\frac{P_{I_i I_t}(m,n,\mathbf{r})}{P_{I_i}(m,\mathbf{r}) P_{I_t}(n)}\right)$$

where $P_{I_i I_t}$ is the joint probability distribution between $I_i(\mathbf{w}_m(\mathbf{p};\mathbf{r}))$ and $I_t(\mathbf{p})$. P_{I_i} and P_{I_t} are marginal distributions of $I_i(\mathbf{w}_m(\mathbf{p};\mathbf{r}))$ and $I_t(\mathbf{p})$, respectively. They are estimated using normalized histograms.

The main purpose of NCC and MI based visual tracking is to find $\mathbf{r}$ vector which maximizes the similarity value between $I_i(\mathbf{w}_m(\mathbf{p};\mathbf{r}))$ and $I_t(\mathbf{p})$ using Newton optimization.

According to Newton optimization, derivation of the similarity function, $s(x)$, equals to zero at the extremum point. For this purpose, the Taylor series representation of $s(x)$ with respect to small increments of x, δx, is computed:

$$s(x+\delta x) \approx s(x) + \delta x s'(x) + \frac{\delta x^2}{2} s''(x) + HOT$$
$$s'(x+\delta x) = s'(x) + \delta x s''(x) = 0$$

The equation above is valid for multiple dimensions ($s : \mathbf{R}^n \mapsto \mathbf{R}$). In that case, gradient vector ($\mathbf{g}$) and Hessian ($\mathbf{H}$) matrix can be replaced with the first and second derivatives of $s(x)$, respectively. Also, δx can be replaced with small increments of motion parameters, $\Delta\mathbf{r}$. Then, the motion parameters can be calculated using gradient and Hessian as follows:

$$\Delta\mathbf{r} = -\mathbf{H}^{-1}\mathbf{g} \quad (2)$$

Computation of gradient vector and Hessian matrix for NCC and MI similarity functions can be found in [18] and [19], respectively. Parameters, $\mathbf{r}$, are iteratively calculated. Before iterations start, $\mathbf{H}$ and its inverse are computed. At each iteration, $\mathbf{g}$ is updated. Then, $\Delta\mathbf{r}$ is calculated using (2) and it is accumulated to find all motion parameters ($\mathbf{r} \leftarrow \mathbf{r} + \Delta\mathbf{r}$). Iterations are repeated until $\Delta\mathbf{r}$ becomes smaller than predefined threshold value to break iterations or number of iterations reaches predefined maximum iteration number.

B. Template Update Strategy

Template update strategy with drift correction is used to update the needle templates[20]. Schematic diagram of visual tracking using this strategy is illustrated in Fig. 3. After an image pair is registered, output image is registered with the master template of the needle. Then, template image is updated with the registration output. Thus, registration error is so minimized that template is not drifting along the needle path [13]. Initially, master template is the first needle template in the beginning of the tracking and it is updated in every 15 frames. Fig. 4 shows the successful needle tip tracking using this strategy in ex-vivo phantom.

C. Data Fusion

After an image pair is registered, there would be a residue error which is called registration error. In this study, outputs of the visual tracking using NCC and MI are fused to reduce the registration error. This error is relatively small and it can be minimized using the template update strategy with drift correction. Only one of the visual tracking outputs is used to minimize this error. If outputs of both visual tracking methods are fused, registration error can be further reduced, and tracking can be more accurate. In order to fuse two outputs, the Kalman filter is used [21]. $\mathbf{p}_{NCC}$ and $\mathbf{p}_{MI}$ are vectors which contain visual tracking outputs of NCC and MI, which are obtained in parallel. Then, difference between

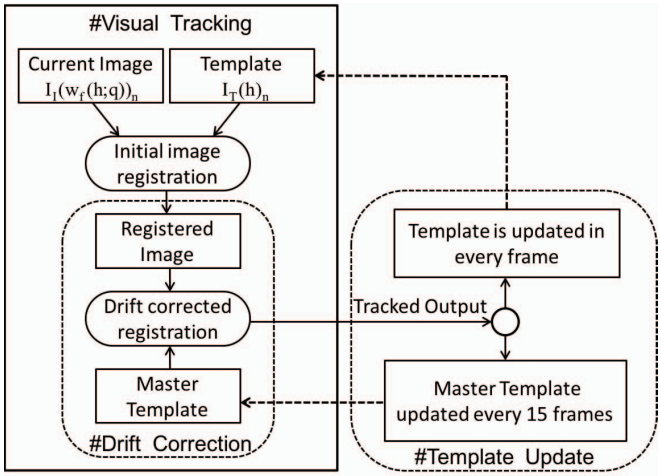

Fig. 3: Schematic diagram of visual tracking using the template update strategy with drift correction.

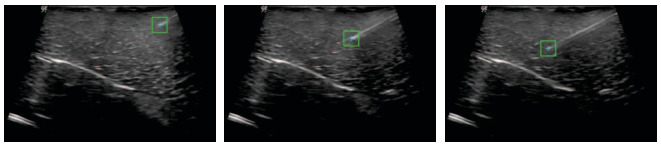

(a) Frame #1 (b) Frame #50 (c) Frame #104

Fig. 4: Results of needle tip tracking in ex-vivo phantom.

$\mathbf{p}_{MI}$ and $\mathbf{p}_{NCC}$ are delivered to the Kalman filter to estimate the registration noise, $\mathbf{e}_{KF}$. Finally, $\mathbf{e}_{KF}$ is subtracted from $\mathbf{p}_{MI}$ to minimize the registration error and fused output, $\mathbf{p}_f$, is obtained. Schematic diagram of the data fusion process is depicted in Fig. 5.

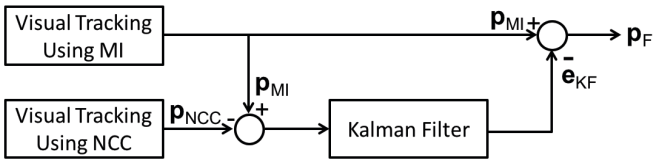

Fig. 5: Schematic diagram of data fusion process.

III. Target Tracking

During insertion, the target tissue also moves due to the probe motion or stick-slip forces [12]. In order to collect samples from the correct place, target also has to be tracked. Visual tracking, which is used to track the needle tip, can also be used to track the target, since the US image contains the motion information of the target as well (see Fig. 1). Target tracking can be divided into two sections: moving target tracking and deformable target tracking. In the rest of this section, these are explained in detail.

A. Small and Moving Target Tracking

During insertion, patients inhale and the target region moves with the breathing motion. Also, the US probe can be moved time to time to image the needle and the target. Small and moving targets can be tracked in the same way that the needle tip is tracked. In order to track small and moving targets, an affine motion model is used. Both non-rigid and rigid transformations in target tissue can be tracked using this motion model. If a more complex motion model is used, tracking might be unsuccessful because US images suffer from low signal-to-noise ratio [22]. Thus, complex motion models can reduce the robustness of tracking.

During target tracking experiments, US probe was vertically moved with respect to target. Also, US probe was pushed and pulled towards phantom to mimic the patient breathing. In these cases, target was successfully tracked using the affine model. Fig. 6 shows the results of successful target tracking using affine motion model. Needle tip and small target are simultaneously tracked in real-time.

B. Deformable Target Tracking

An example motion analysis of deformable phantom while needle is inserting is shown in Fig. 7. In this case, complete tissue should be tracked for accurate target tracking. Like small and moving targets, visual tracking methods can be used to track the deformable tissue. But, different motion model should be used.

In order to express the motion of the deformable tissue, thin plate spline (TPS) deformable motion model is used. In the literature, it was previously used to track objects or targets in both photometric and medical images [23]. TPS is a radial basis function and interpolates n target points (x', y') using given n control points $(\widehat{x}, \widehat{y})$ $((\widehat{x}, \widehat{y}) \mapsto (x', y'))$. It minimizes the bending energy using an approximation function $f : R^2 \mapsto R$:

$$E_f = \iint_{R^2} \left(\frac{\partial^2 f}{\partial x^2}\right)^2 + 2\left(\frac{\partial^2 f}{\partial x \partial y}\right)^2 + \left(\frac{\partial^2 f}{\partial y^2}\right)^2 \partial x \partial y$$

The interpolated coordinate of a point in a plane (x, y) can be calculated using TPS, such that:

$$f(x,y) = \begin{bmatrix} a_0 & a_1 \\ a_3 & a_4 \end{bmatrix} \begin{bmatrix} x \\ y \end{bmatrix} + \begin{bmatrix} a_2 \\ a_5 \end{bmatrix} + \sum_{i=1}^{n} \begin{bmatrix} w_x^i \\ w_y^i \end{bmatrix} U(\|(\widehat{x}_i, \widehat{y}_i) - (x,y)\|) \quad (3)$$

where

$$U(r) = r^2 \log r$$

and $(a_0, ..., a_5)$ are the affine parameters, (w_x, w_y) are weights of a control point in (x, y) location.

TPS motion parameters $\mathbf{a} = (a_0, ..., a_5)$ and $\mathbf{w} = (w_x, w_y)$ can be obtained by solving the linear system:

$$\begin{bmatrix} \mathbf{w} \\ \mathbf{a} \end{bmatrix} = \begin{bmatrix} \mathbf{K} & \mathbf{P} \\ \mathbf{P}^T & \mathbf{O} \end{bmatrix}^{-1} \begin{bmatrix} \mathbf{V} \\ \mathbf{0} \end{bmatrix}^T$$

where

$$\mathbf{K} = \begin{bmatrix} 0 & U(r_{12}) & \dots & U(r_{1n}) \\ U(r_{21}) & 0 & \dots & U(r_{2n}) \\ \vdots & \vdots & \ddots & \vdots \\ U(r_{n1}) & U(r_{n2}) & \dots & 0 \end{bmatrix}, \mathbf{P} = \begin{bmatrix} 1 & \widehat{x_1} & \widehat{y_1} \\ 1 & \widehat{x_2} & \widehat{y_2} \\ \vdots & \vdots & \vdots \\ 1 & \widehat{x_n} & \widehat{y_n} \end{bmatrix},$$

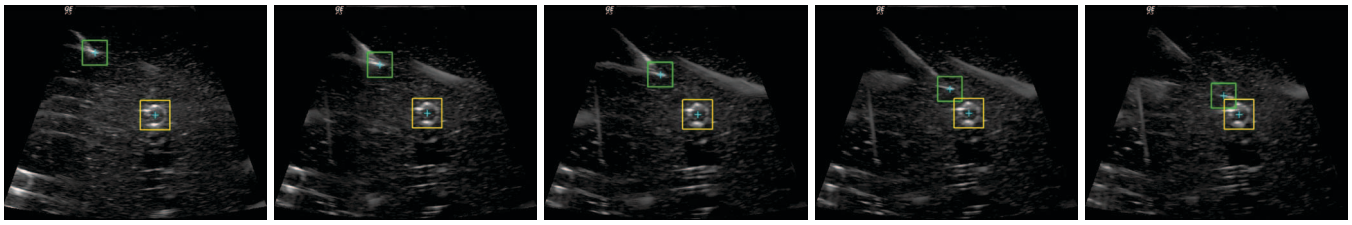

(a) Frame #2 (b) Frame #76 (c) Frame #124 (d) Frame #165 (e) Frame #223

Fig. 6: Results of simultaneous needle tip and moving target tracking in agar-gelatine phantom.

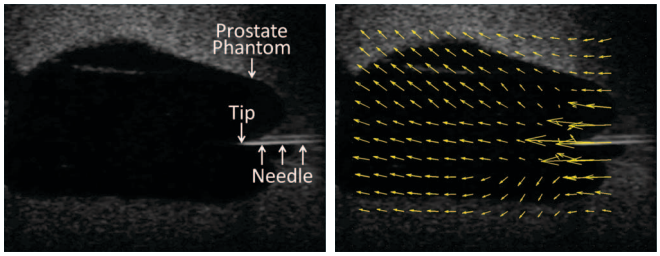

(a) Current Frame (b) Vector Field

Fig. 7: Motion analysis of deformable prostate phantom while needle is inserting. (a) Current US frame. (b) Optical vector field is overlaid onto current frame.

$$\mathbf{V} = \begin{bmatrix} x'_1 & x'_2 & \dots & x'_n \\ y'_1 & y'_2 & \dots & y'_n \end{bmatrix}.$$

where $r_{ij} = \|(\widehat{x}_i, \widehat{y}_i) - (\widehat{x}_j, \widehat{y}_j)\|$. $\mathbf{O}$ and $\mathbf{0}$ are 3×3 and 2×3 zero matrices, respectively.

Equation (3) is used to express the motion of deformable tissue. During the visual tracking, motion parameters which minimize difference between current and template ($\mathbf{r} = (a_0, ..., a_5, w_x^T, w_y^T)$) are calculated and coordinates of target region are obtained.

Fig. 8 shows the results of deformable tissue tracking using TPS motion model while needle is inserting into prostate phantom. Four control points are selected and 2D 15×15 nodes are created to show the deformation. The needle tip and the target are simultaneously tracked in the deformable tissue. Results are shown in Fig. 9. Despite poor quality frames, needle tip and deformable tissue were successfully tracked. Also note that if only target region is visually tracked, tracking will fail because target region does not contain any texture information.

IV. Visual Servoing

Visual servoing is to keep the target in image plane by moving the vision sensor. In our case, needle tip is kept in the US image plane by moving the US probe while following the motion of the needle tip. A PID controller is designed to servo the US probe [24]. PID gains are tuned for fast steady state response and to prevent overshoots. The center of image is chosen as the set point. The error between needle tip location and the set point is multiplied with corresponding PID gains until needle tip is reached to image plane center.

V. Experiments

A. Experimental Setup

In the experiments, a GE LOGIQ P5 2D US machine with a GE 11L linear 2D US probe were used. The size of the acquired US images was 640×480 pixels, which provides 163.3 μm/pixel resolution. They were transferred from the US machine to computer using a frame grabber (EURESYS PICOLO HD3G) at 15 frames per second. In order to test the proposed needle tip and target tracking methods, lamb meat, chicken breast, distilled water, and four different phantoms (water-ethanol mixture, gelatine, agar, agar-gelatine) were used. Meats are embedded into gelatine to fix them. Also, olives, pipettes, and water filled balloons were embedded into phantoms to simulate cysts, veins, and deformable tissues. Phantoms were prepared according to recipes in [11]. 18G×15cm biopsy needles (Gallini Medical Devices) and a 12G×25cm stainless steel shafts were used for needle insertion experiments.

2D US probe was mounted on to a 6-DOF robotic arm (KUKA KR 6 R9000 sixx), and needle was inserted using a 5-DOF needle insertion robot [25]. 11.4 mm diameter optical markers were attached onto the needle mechanism and the US probe to track the motion and measure accuracy of proposed methods. OptiTrack motion capture system was used to capture marker motion. The experimental setup is shown in Fig. 10.

B. Experimental Results

1) Execution Time: Proposed visual tracking methods were implemented in both MATLAB and C++ using OpenCV library; and ran on a 64-bit Windows 7 workstation (Intel Xeon E5-2620 CPU running at 2 GHz and 32 GB RAM). During the experiments, size of the template images was 61×61. The maximum iteration number and threshold value for breaking the iteration loop were set 50 and 0.01, respectively. Execution times of visual tracking are tabulated in Table I. Execution time of visual tracking using NCC and MI was reduced twenty folds in C++ implementation. Thus, the target and the needle were simultaneously tracked in real-time.

2) Accuracy of needle tip tracking: In order to evaluate the proposed needle tip tracking an optical tracking system was used. Experiments were carried out in a water tank. First, 2D US was calibrated in 3D space using proposed calibration method in [26]. In the experiments, needle was

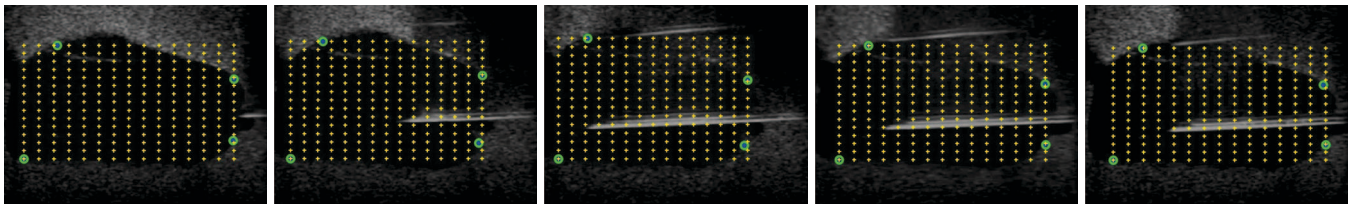

(a) Frame #1 (b) Frame #68 (c) Frame #137 (d) Frame #168 (e) Frame #200

Fig. 8: Results of deformable tissue tracking using TPS. Control points are shown with 'o' and '+' indicates nodes.

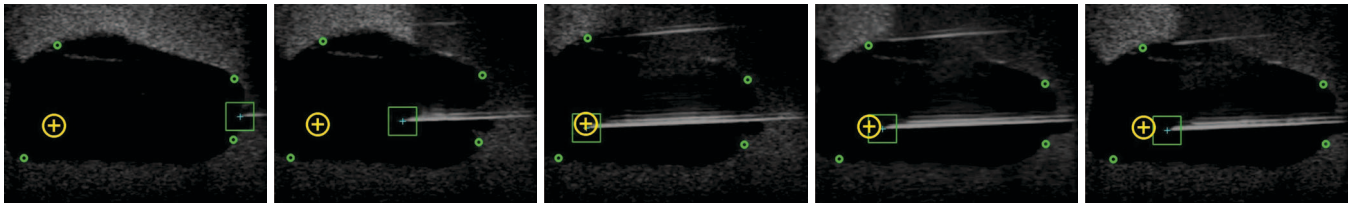

(a) Frame #1 (b) Frame #68 (c) Frame #137 (d) Frame #168 (e) Frame #168

Fig. 9: Results of simultaneous needle tip and target tracking in deformable prostate phantom. Target is shown with '⊕' and '+' indicates the needle tip. The frame sequences were downloaded from https://youtu.be/H5OSEKag42w and they are affected by the H264 coding artifacts.

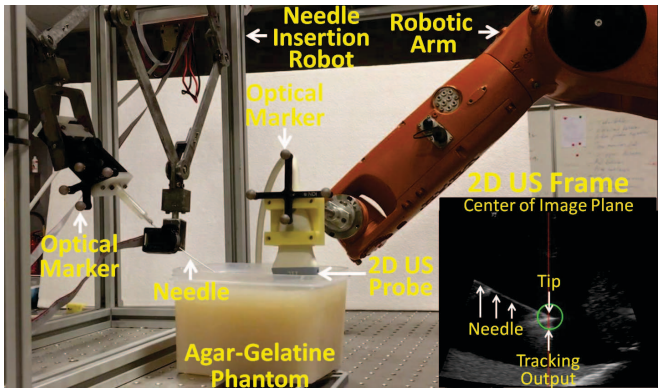

Fig. 10: View of the experimental setup.

TABLE I: Comparison of execution times

Method	Execution Time [ms]	
	MATLAB	C++
Visual Tracking using NCC	660 ± 170	28 ± 11
Visual Tracking using MI	1005 ± 220	42 ± 6

inserted and retracted at different angles and velocities. Needle tip coordinates were simultaneously obtained using both optical tracking and visual tracking. Then, Euclidian distance between them was calculated for each frame. In total, 8296 frames were acquired. The errors are plotted in box representation and it is shown in Fig. 11. Errors of proposed needle tip tracking methods are below 0.4 mm. Fusion of NCC and MI reduces tracking error over 15%, and the mean error of the fused information is 0.215 mm. One way ANOVA was used to test statistical significance of the results given in Fig. 11, and they were found to be significantly different ($F(2, 24885) = 8675.9$, $p = .000$).

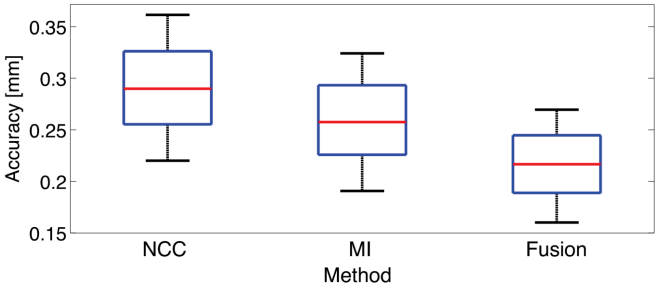

Fig. 11: Tracking error of the proposed needle tip tracking method using NCC, MI, and fusion of NCC and MI.

3) Accuracy of visual servoing: In order to evaluate the accuracy of visual servoing, needle was inserted using an insertion robot and 2D US probe was attached to a robotic arm. These experiments were performed using water tank and different types of phantoms including gelatine, agar, and agar-gelatine based phantoms. Thus, needle tip was servoed in both solid and liquid mediums. The insertion robot was used to insert the needle both with a manual control and a predefined sinusoidal wave.

The needle tip position was tracked using the proposed tracking method. The needle tip position was used as reference signal to a PID controller which sends reference signal to the robotic arm which was moving the US probe. PID gains were tuned to keep the needle tip position within 3 mm of the image plane center. The accuracy was evaluated using the optical tracking system. The motion of the needle tip and the US probe were simultaneously recorded and then

error was calculated. The motion are plotted in the left of Fig. 12. Error between the needle tip position and image plane center over time is also plotted and it is illustrated on the right of Fig. 12. RMS error was calculated as 2.13 mm. This accuracy is in the sufficient range for visual servoing of the needle tip.

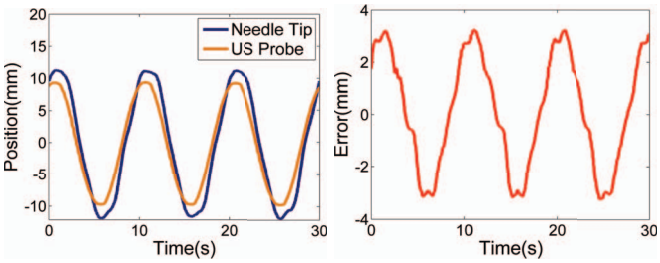

Fig. 12: Left side image shows data from optical tracking system and right side image shows error over time between image center and the needle tip.

VI. Conclusion

This study presents visual tracking of needle tip and targets for 2D US guided robotic percutaneous interventions. The main contribution to the literature is that needle tip, moving, and deformable targets are simultaneously tracked using NCC and MI similarity functions. Also, visual tracking outputs of NCC and MI are fused to minimize the registration error. The proposed tracking method was applied to a 2D US guided biopsy robotic system, and needle tip and target were tracked during insertion. The experiments were carried out in different types of mediums. Heterogenous and deformable phantoms were especially produced to show that proposed methods can track the needle tip and targets in challenging conditions. Execution times of proposed tracking methods were substantially reduced in C++ implementation so needle and target were simultaneously tracked in real-time. Accuracy of proposed tracking methods were evaluated using an optical tracking system. Experimental results showed that accuracies of proposed tracking methods are in sufficient interval and needle and target can be tracked simultaneously in 2D US guided percutaneous needle procedures in real-time using the proposed tracking methods.

References

[1] H. T. Şen, A. Cheng, K. Ding, E. Boctor, J. Wong, I. Iordachita, and P. Kazanzides, "Cooperative control with ultrasound guidance for radiation therapy," *Frontiers in Robotics and AI*, vol. 3, p. 49, 2016.

[2] K. Mathiassen, D. Dall'Alba, R. Muradore, P. Fiorini, and O. J. Elle, "Robust real-time needle tracking in 2D ultrasound images using statistical filtering," *IEEE Transactions on Control Systems Technology*, vol. PP, no. 99, pp. 1–13, 2016.

[3] E. Ayvali and J. P. Desai, "Optical flow-based tracking of needles and needle-tip localization using circular hough transform in ultrasound images," *Annals of biomedical engineering*, vol. 43, no. 8, pp. 1828–1840, 2015.

[4] Y. Zhao, A. Bernard, C. Cachard, and H. Liebgott, "Biopsy needle localization and tracking using roi-rk method," in *Abstract and Applied Analysis*, vol. 2014. Hindawi Publishing Corporation, 2014.

[5] P. Chatelain, A. Krupa, and M. Marchal, "Real-time needle detection and tracking using a visually served 3D ultrasound probe," in *Proceedings of the IEEE International Conference on Robotics and Automation (ICRA)*, no. 2, May 2013, pp. 1668–1673.

[6] P. Chatelain, A. Krupa, and N. Navab, "3D ultrasound-guided robotic steering of a flexible needle via visual servoing," in *IEEE Int. Conf. on Robotics and Automation, ICRA'15*.

[7] G. J. Vrooijink, M. Abayazid, S. Patil, R. Alterovitz, and S. Misra, "Needle path planning and steering in a three-dimensional non-static environment using two-dimensional ultrasound images," *The International journal of robotics research*, p. 0278364914526627, 2014.

[8] L. Royer, M. Marchal, A. Le Bras, G. Dardenne, and A. Krupa, "Real-time tracking of deformable target in 3D ultrasound images," in *2015 IEEE International Conference on Robotics and Automation (ICRA)*. IEEE, 2015, pp. 2430–2435.

[9] L. Royer, M. Babel, and A. Krupa, "Non-rigid target tracking in 2D ultrasound images using hierarchical grid interpolation," in *SPIE Medical Imaging*. International Society for Optics and Photonics, 2014, pp. 90 343O–90 343O.

[10] M. Kaya and O. Bebek, "Needle localization using gabor filtering in 2D ultrasound images," in *Robotics and Automation (ICRA), 2014 IEEE International Conference on*. IEEE, 2014, pp. 4881–4886.

[11] ——, "Gabor filter based localization of needles in ultrasound guided robotic interventions," in *Imaging Systems and Techniques (IST), 2014 IEEE International Conference on*. IEEE, 2014, pp. 112–117.

[12] M. Kaya, E. Senel, A. Ahmad, O. Orhan, and O. Bebek, "Real-time needle tip localization in 2D ultrasound images for robotic biopsies," in *Advanced Robotics (ICAR), 2015 International Conference on*. IEEE, 2015, pp. 47–52.

[13] M. Kaya, E. Senel, A. Ahmad, and O. Bebek, "Visual tracking of biopsy needles in 2D ultrasound images," in *Proceedings of the IEEE International Conference on Robotics and Automation (ICRA)*, 2016.

[14] B. D. Lucas and T. Kanade, "An iterative image registration technique with an application to stereo vision." in *IJCAI*, vol. 81, no. 1, 1981, pp. 674–679.

[15] S. Baker and I. Matthews, "Lucas-kanade 20 years on: A unifying framework," *International journal of computer vision*, vol. 56, no. 3, pp. 221–255, 2004.

[16] J. P. Pluim, J. A. Maintz, and M. A. Viergever, "Mutual-information-based registration of medical images: a survey," *IEEE transactions on medical imaging*, vol. 22, no. 8, pp. 986–1004, 2003.

[17] G. P. Penney, J. Weese, J. A. Little, P. Desmedt, D. L. Hill, *et al.*, "A comparison of similarity measures for use in 2-d-3-d medical image registration," *IEEE transactions on medical imaging*, vol. 17, no. 4, pp. 586–595, 1998.

[18] R. Richa, R. Sznitman, and G. Hager, "Robust similarity measures for gradient-based direct visual tracking," The Johns Hopkins University, Tech. Rep., 2012.

[19] A. Dame and E. Marchand, "Second-order optimization of mutual information for real-time image registration," *IEEE Transactions on Image Processing*, vol. 21, no. 9, pp. 4190–4203, 2012.

[20] I. Matthews, T. Ishikawa, and S. Baker, "The template update problem," *IEEE Transactions on Pattern Analysis & Machine Intelligence*, no. 6, pp. 810–815, 2004.

[21] D. Roetenberg, P. J. Slycke, and P. H. Veltink, "Ambulatory position and orientation tracking fusing magnetic and inertial sensing," *IEEE Trans. on Biomedical Engineering*, vol. 54, no. 5, pp. 883–890, 2007.

[22] F. P. Oliveira and J. M. R. Tavares, "Medical image registration: a review," *Computer methods in biomechanics and biomedical engineering*, vol. 17, no. 2, pp. 73–93, 2014.

[23] R. Richa, P. Poignet, and C. Liu, "Three-dimensional motion tracking for beating heart surgery using a thin-plate spline deformable model," *The International Journal of Robotics Research*, vol. 29, no. 2-3, pp. 218–230, 2010.

[24] S. Hutchinson, G. D. Hager, and P. I. Corke, "A tutorial on visual servo control," *IEEE transactions on robotics and automation*, vol. 12, no. 5, pp. 651–670, 1996.

[25] S. O. Orhan, M. C. Yildirim, and O. Bebek, "Design and modeling of a parallel robot for ultrasound guided percutaneous needle interventions," in *Industrial Electronics Society, IECON 2015-41st Annual Conference of the IEEE*. IEEE, 2015, pp. 005 002–005 007.

[26] A. Ahmad, M. C. Cavusoglu, and O. Bebek, "Calibration of 2D ultrasound in 3D space for robotic biopsies," in *Advanced Robotics (ICAR), 2015 International Conference on*. IEEE, 2015, pp. 40–46.